SUPPORTING INFORMATION

DOI: 10.1039/x0xx00000x

Cononsolvency in the 'drunken' state: Thermoresponsiveness of a new acrylamide copolymer in water-alcohol mixtures

Niklas Lucht, Steffen Eggers, Volker Abetz*

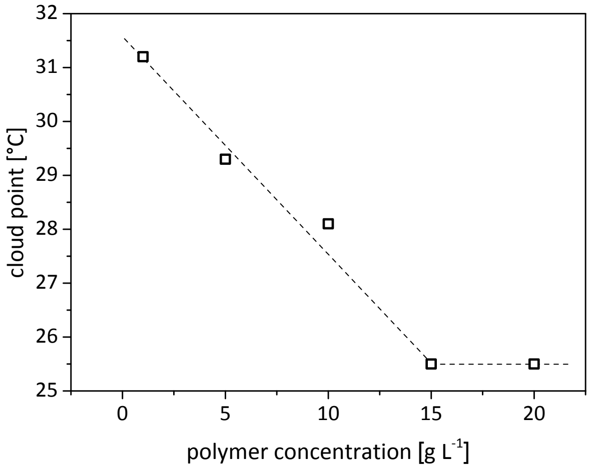

Figure S1: Cloud point of poly[*N*-acryloylpiperidine$_{42}$-*random*-*N*-acryloylpyrrolidine$_{58}$] in dependence on the polymer concentration in water. The minimal cloud point (lower critical solution temperature) is reached at a concentration of 15 g L^{-1}. The dashed line is supposed to guide the eye and is no mathematical fit function.

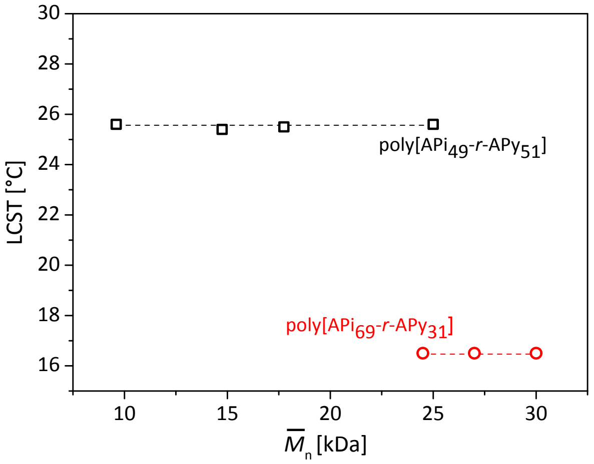

Figure S2: Lower critical solution temperature (LCST) in dependence on the number average molecular weight ($\overline{M}_n$) of two different poly[*N*-acryloylpiperidine-*random*-*N*-acryloylpyrrolidine] (poly[APi$_x$-*r*-APy$_y$]) copolymers with different compositions (indices indicate molar fractions). A molecular weight independence between 10 kDa and 30 kDa can be clearly seen.

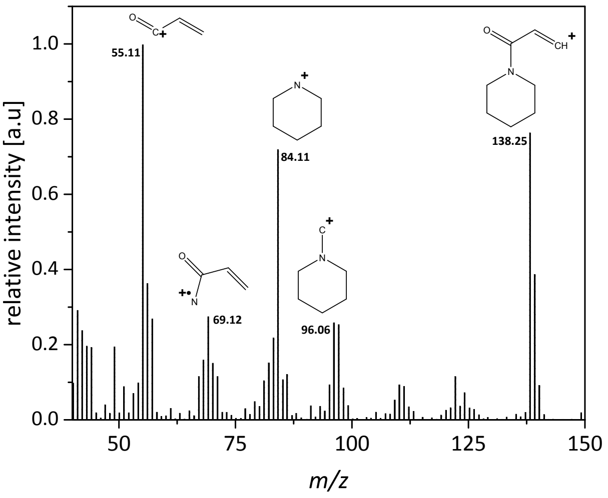

Figure S3: Electron ionisation mass spectrum of the monomer *N*-acryloylpiperidine with indicated molecule fragments.

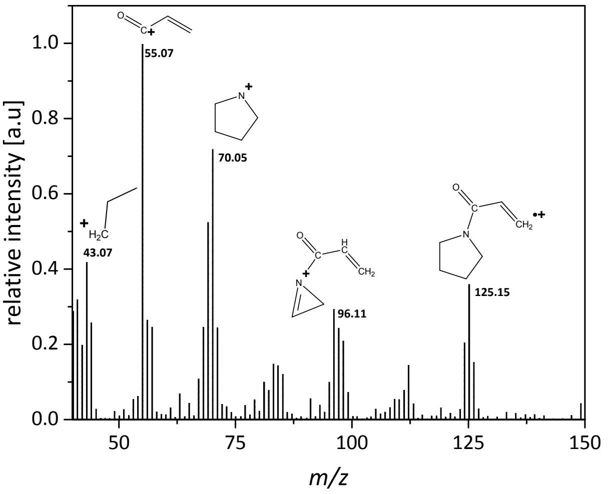

Figure S4: Electron ionisation mass spectrum of the monomer *N*-acryloylpyrrolidine with indicated molecule fragments.

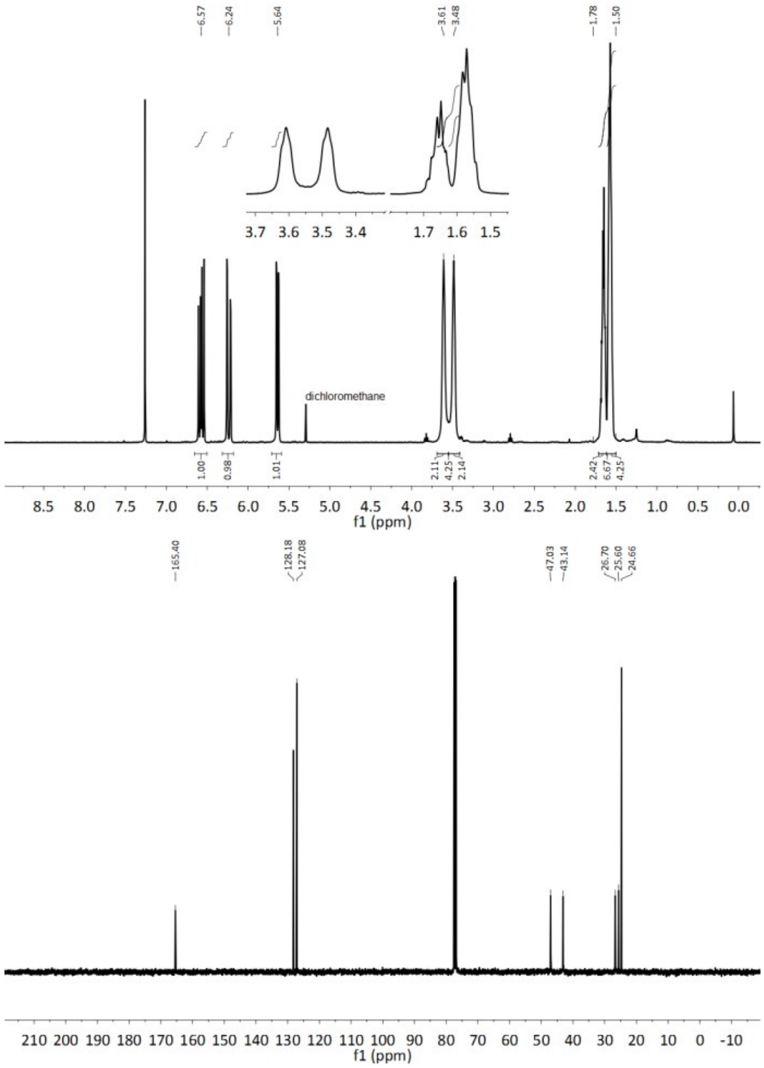

Figure S5: ^{1}H-NMR (top) and ^{13}C-NMR spectrum (bottom) of *N*-acryloylpiperidine in $CDCl_3$.

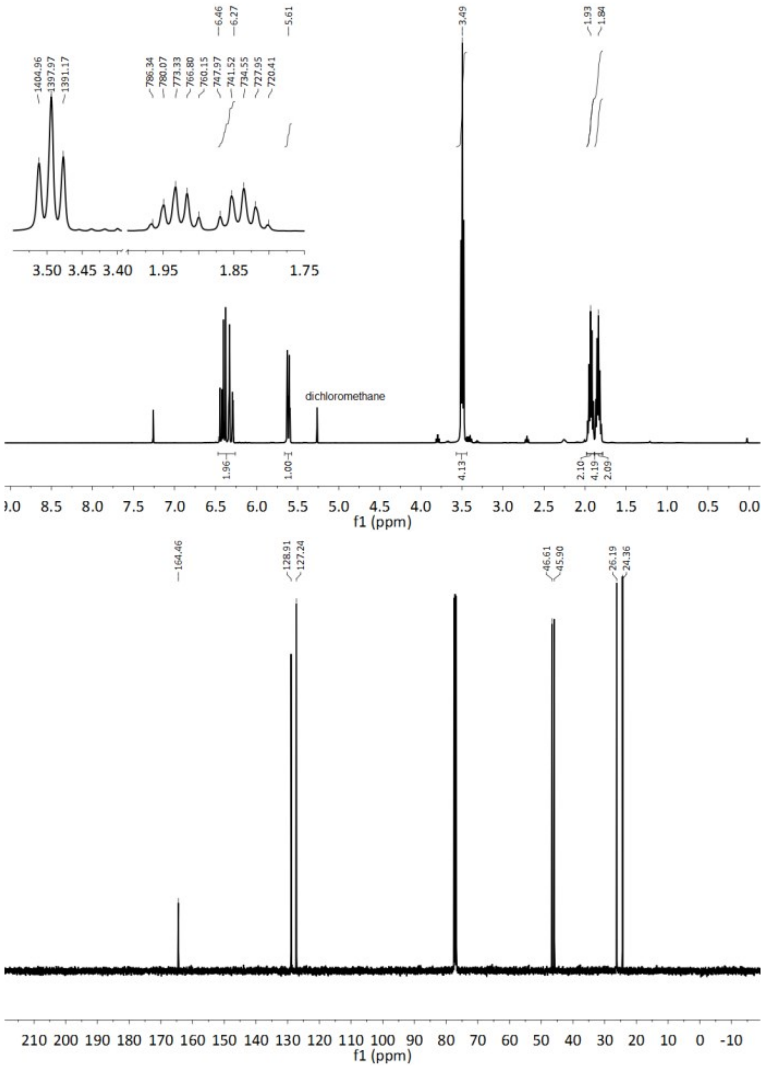

Figure S6: ^{1}H-NMR (top) and ^{13}C-NMR spectrum (bottom) of *N*-acryloylpyrrolidine in $CDCl_3$.

Calculation of the Monomer Conversion

$$\text{monomer conversion} = 1 - \frac{I_{5.64} \times n_{\mathrm{DMF}}}{I_{\mathrm{DMF}} \times n_{0,\mathrm{APi+APy}}}. \quad \text{(Equation S1)}$$

The monomer conversion was calculated using Equation S1 with $I_{5.64}$ being the total residual monomer proton intensity, I_{DMF} being the carbonyl peak intensity of *N,N*-dimethylformamide (DMF) as an internal standard, $n_{0,\mathrm{Api+Apy}}$ being the total initial molar amount of monomer and n_{DMF} being the added molar amount of DMF.

Temperature-dependent Dynamic Light Scattering

Experimental Procedure

DLS measurements were conducted on an ALV/CSG-3 Compact Goniometer-System using a ALV/LSE-5003 Multiple Tau Digital Correlator working with pseudo cross correlation and the ALV Digital Correlator Software 3.0. The measuring angle was set to 90° for all measurements, every single measurement was conducted for 30 s. As light source, a Nd:YAG laser emitting at 532 nm was used. The sample vials consisted of quartz glass and were placed into a measurement cell filled with toluene. Prior to measurement, the sample solutions were filtered through a microporous filter (average pore diameter = 200 nm) made from regenerated cellulose.

Temperature-dependent measurements were conducted in temperature steps of 0.5 °C with one measurement per temperature. The measurements were started 10 °C below the expected cloud point (if possible) and ended at a temperature of 5 °C above the expected cloud point. It was always measured upwards and downwards to check reversibility of the investigated transition. The toluene bath and therefore the samples were tempered by a Julabo F25 thermostat working with a mixture of water and ethylene glycol and delivering a temperature accuracy of 0.01 °C. Each set temperature was stabilized for 3 min prior to measurement.

The viscosity and refractive index of the solutions were automatically corrected with temperature according to tabulated values of the solvents, i.e. water, methanol/water, ethanol/water, propan-1-ol/water and propan-2-ol/water.[1-3] For non-tabulated mixtures, i.e. ethane-1,2-diol/water, propane-1,2-diol/water and propane-1,3-diol/water, the viscosity and refractive index were interpolated using tabulated values for the pure solvents.

The diffusion coefficient D ($D = \bar{\Gamma}/q^2$) was calculated automatically by the DLS software from the wave vector q and the averaged relaxation rate $\bar{\Gamma}$ by fitting the field autocorrelation function $g^1(q,t)$ with a cumulant up to second order:

$$\ln\left(g^1(q,t)\right) = \ln A - \bar{\Gamma} \times t + \frac{\mu_2}{2} \times t^2 \text{. (Equation S2)}$$

t: time. A: amplitude. The size dispersity $\frac{\mu_2}{\bar{\Gamma}^2}$ of the particles was calculated from the second moment μ_2.

The hydrodynamic radius (R_h) was estimated from D via the Stokes–Einstein equation. The relative scattering intensity was calculated by dividing the averaged count rate from the two crossed correlators by the monitor value. The relative scattering intensity was then normalized. Number weighted size distributions were obtained by fitting the data with a Contin algorithm.

Discussion

The DLS data (for the graphs, see below) show a high accordance to the turbidimetry data (marked as a dashed red line in the graphs) concerning the cloud point estimation of the analysed solutions. At the respective cloud points, there is an instantaneous and strong increase of the hydrodynamic radius (R_h) from roughly 9–11 nm for the dissolved random coils (according to cumulant analysis) to micrometer-sized aggregates. This sharpness of the transition suggests a high degree of cooperativity of the chain collapse at the cloud point which is quite remarkable as this feature is often dedicated to the ability of the collapsing polymer to form intramolecular hydrogen bonds.[4] In combination with the high degree of reversibility of the phase transition which was observed in DLS (not shown) as well as in turbidimetry, the sharpness of the clouding underlines the stimuli-responsiveness of the systems. The cloud point discrepancy of DLS and turbidimetry is < 0.5 °C in all cases and the cloud points are, if different, higher if being determined by DLS than the ones determined by turbidimetry. This is caused in the temperature step size of 0.5 °C in the DLS experiments, the lower heating rate ($dT/dt \approx 3$ °C h^{-1} in DLS versus $dT/dt \approx 2$ °C min^{-1} in turbidimetry) and the different experimental conditions, as the solutions cannot be stirred during the DLS experiments.

The initial R_h-values for a specific polymer in the different alcohol–water solvent mixtures at temperatures below the cloud point do not differ significantly, indicating that the initial swelling of the polymer coils is similar (the R_h-value includes the size of the diffusing dissolved polymer coil as well as the solvent environment moving together with the polymer coil). From this, hence, no difference in solvent quality can be derived, as opposed to the shift of the cloud points. This could support the theory of Kremer et al. mentioned in the main manuscript, that cononsolvency is not a result of poorer solvent quality but caused in loop formation of the polymer induced by bridging additive molecules.[5,6]

The huge growth of the aggregates to R_h-values of above 1 µm at the cloud point suggests a quantitative collapse of the polymer chains followed by a high degree of aggregation. This finding is supported by the absence of signs of left over dissolved polymer coils in the size distributions obtained by Contin analysis. Moreover, it can be seen from the decreasing scattering intensity plots above the cloud points that the formed aggregates are colloidally unstable and precipitate (not observed in the turbidimetry experiments, probably due to stirring of the colloidal solution and faster cooling after exceeding the cloud point in those experiments). This is very likely a consequence of the rather high polymer concentration of 20 mg mL^{-1} (for lower concentrations of thermoresponsive polymer solutions the formation of so-called mesoglobules, i.e. colloidally stable aggregates, is often observed).[7,8] Such precipitation usually ends up in a decrease of reversibility of the aggregation process due to a kinetic hindrance of the redissolution of the precipitate, especially when the sample cannot be stirred during the experiment. This is, however, not observed in our experiments because the precipitate appears to retain sufficient free volume for the rediffusion of the solvent at temperatures below the cloud point.

To sum up, the temperature-dependent DLS measurements support and supplement the turbidimetry data discussed in the main manuscript. Nevertheless, light scattering methods, besides others, deliver more opportunities for analysing the solution behaviour of the copolymers in the additive–water systems beyond the ones discussed in this section. Just to name one option, (temperature-dependent) static light scattering can be utilised to estimate radii of gyration or aggregation numbers. This is, though, not part of this work.

Figures

In the following, the temperature-dependent R_h-values as well as normalised relative scattering intensity are depicted. Furthermore, exemplary number weighted size distributions obtained via fitting with a Contin algorithm, molar composition of the copolymers as well as volume fraction of the alcohol in the aqueous solvent mixture are included in the graphs. The vertical dashed red line indicates the cloud point estimated by turbidimetry.

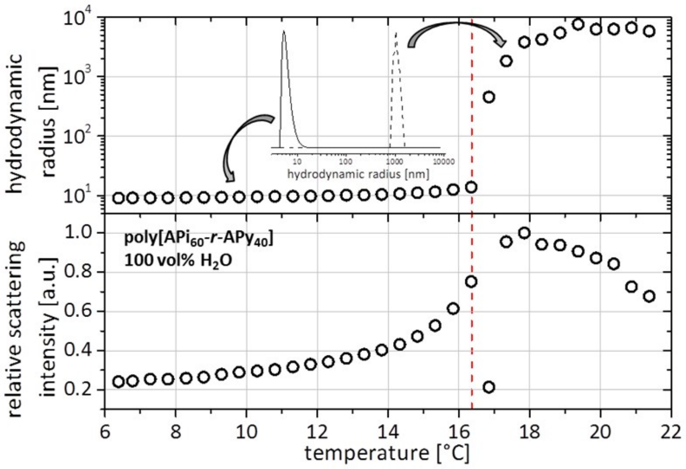

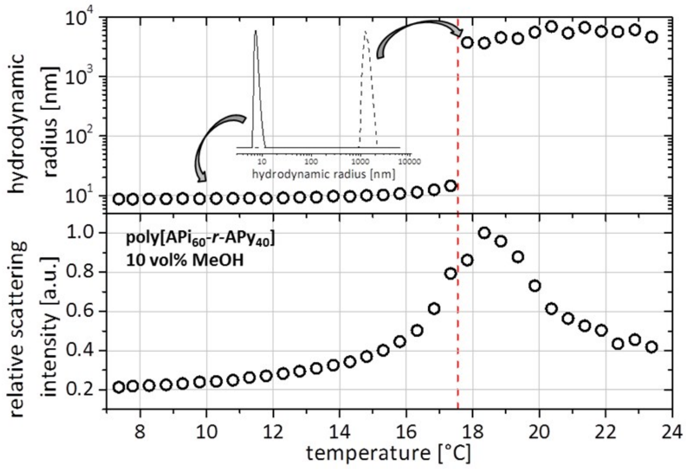
hydrodynamic radius [nm]
10^1
10^2
10^3
10^4
10
100
1000
10000
hydrodynamic radius [nm]
poly[APi$_{60}$-*r*-APy$_{40}$]
10 vol% MeOH
relative scattering intensity [a.u.]
0.2
0.4
0.6
0.8
1.0
8
10
12
14
16
18
20
22
24
temperature [°C]

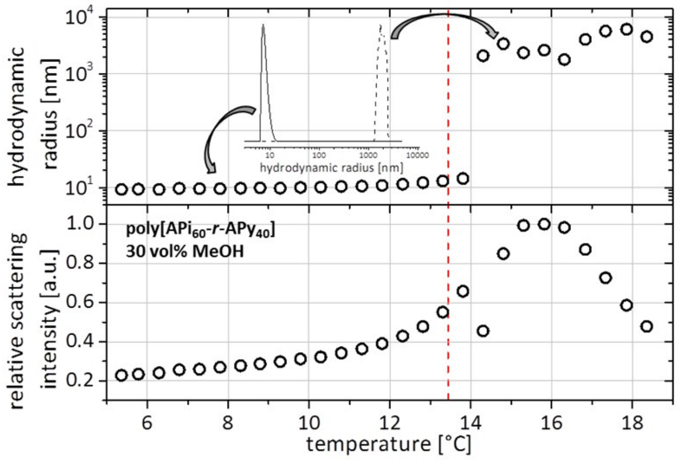
hydrodynamic radius [nm]
10^1
10^2
10^3
10^4
10
100
1000
10000
hydrodynamic radius [nm]
poly[APi$_{60}$-*r*-APy$_{40}$]
30 vol% MeOH
relative scattering intensity [a.u.]
0.2
0.4
0.6
0.8
1.0
6
8
10
12
14
16
18
temperature [°C]

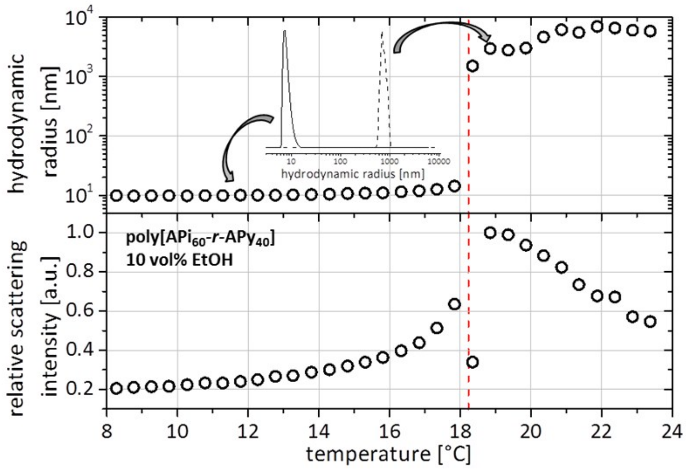
hydrodynamic radius [nm]
10^1
10^2
10^3
10^4
10
100
1000
10000
hydrodynamic radius [nm]
poly[APi$_{60}$-*r*-APy$_{40}$]
10 vol% EtOH
relative scattering intensity [a.u.]
0.2
0.4
0.6
0.8
1.0
8
10
12
14
16
18
20
22
24
temperature [°C]

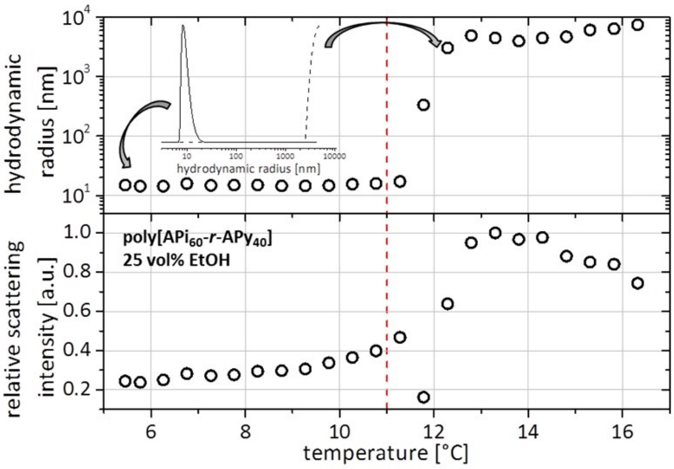
hydrodynamic radius [nm]
10^1
10^2
10^3
10^4
10
100
1000
10000
hydrodynamic radius [nm]
relative scattering intensity [a.u.]
0.2
0.4
0.6
0.8
1.0
poly[APi$_{60}$-*r*-APy$_{40}$]
25 vol% EtOH
6
8
10
12
14
16
temperature [°C]

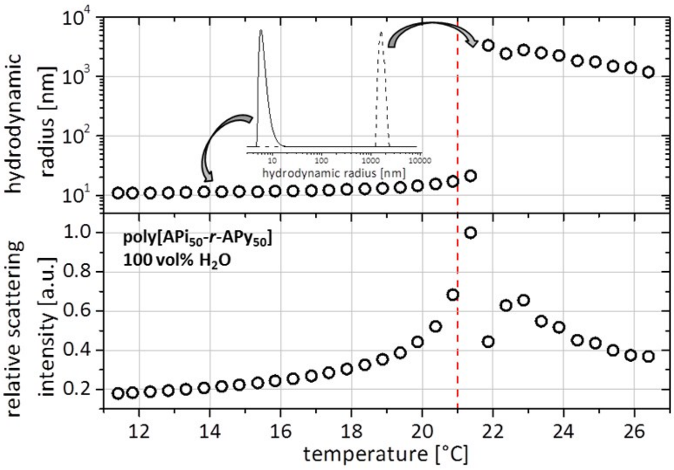
hydrodynamic radius [nm]
10^1
10^2
10^3
10^4
10
100
1000
10000
hydrodynamic radius [nm]
relative scattering intensity [a.u.]
0.2
0.4
0.6
0.8
1.0
poly[APi$_{50}$-*r*-APy$_{50}$]
100 vol% H$_2$O
12
14
16
18
20
22
24
26
temperature [°C]

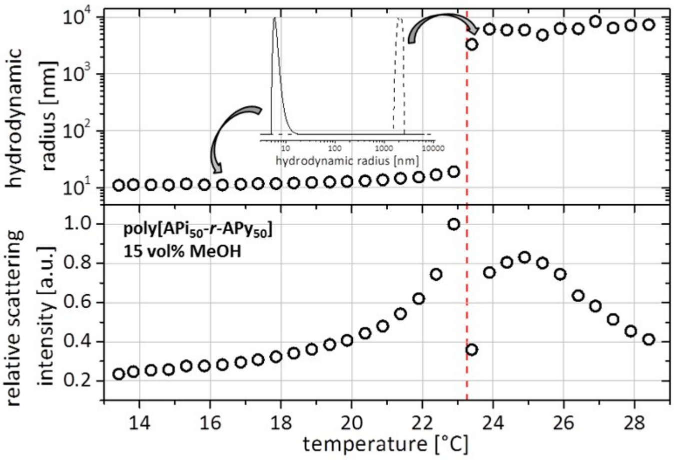
hydrodynamic radius [nm]
10^1
10^2
10^3
10^4
10
100
1000
10000
hydrodynamic radius [nm]
relative scattering intensity [a.u.]
0.2
0.4
0.6
0.8
1.0
poly[APi$_{50}$-*r*-APy$_{50}$]
15 vol% MeOH
14
16
18
20
22
24
26
28
temperature [°C]

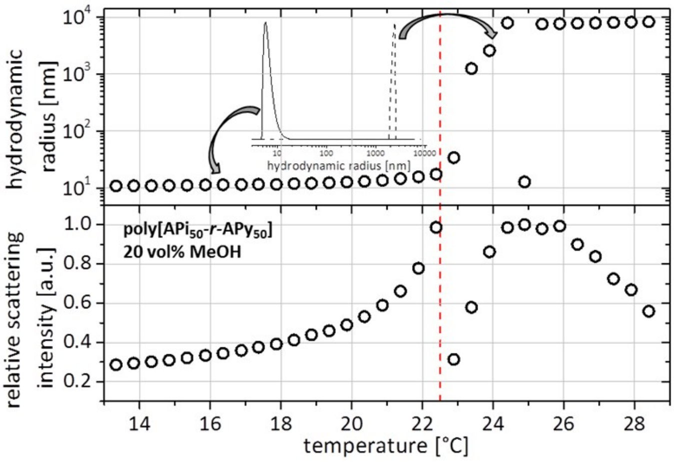
hydrodynamic radius [nm]
10^4
10^3
10^2
10^1
hydrodynamic radius [nm]
10
100
1000
10000
poly[APi_{50}-r-APy_{50}]
20 vol% MeOH
relative scattering intensity [a.u.]
1.0
0.8
0.6
0.4
0.2
14
16
18
20
22
24
26
28
temperature [°C]

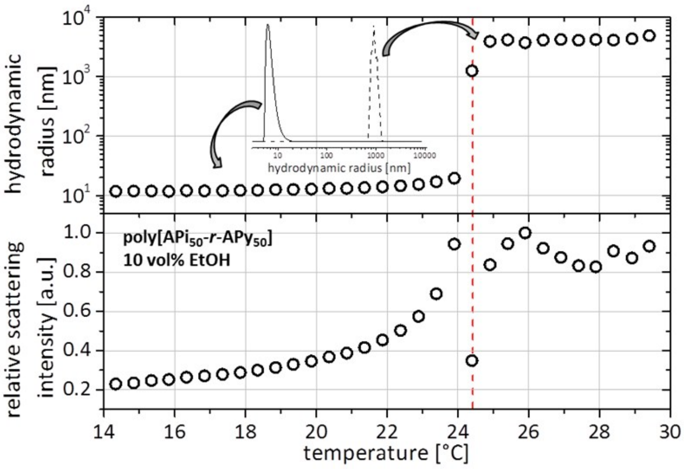
hydrodynamic radius [nm]
10^4
10^3
10^2
10^1
hydrodynamic radius [nm]
10
100
1000
10000
poly[APi_{50}-r-APy_{50}]
10 vol% EtOH
relative scattering intensity [a.u.]
1.0
0.8
0.6
0.4
0.2
14
16
18
20
22
24
26
28
30
temperature [°C]

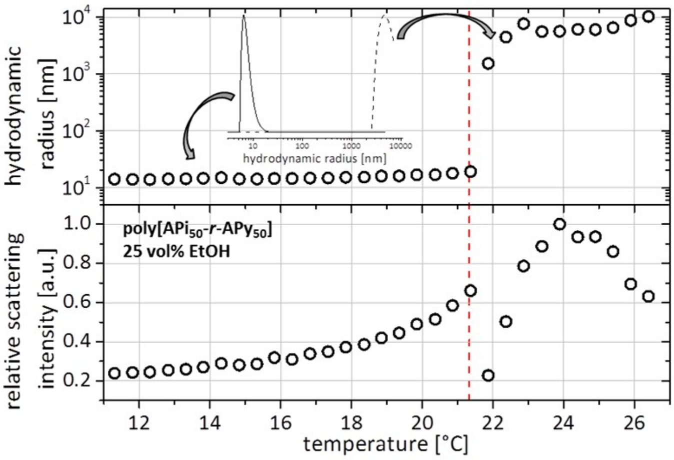
hydrodynamic radius [nm]
10^4
10^3
10^2
10^1
hydrodynamic radius [nm]
10
100
1000
10000
poly[APi_{50}-r-APy_{50}]
25 vol% EtOH
relative scattering intensity [a.u.]
1.0
0.8
0.6
0.4
0.2
12
14
16
18
20
22
24
26
temperature [°C]

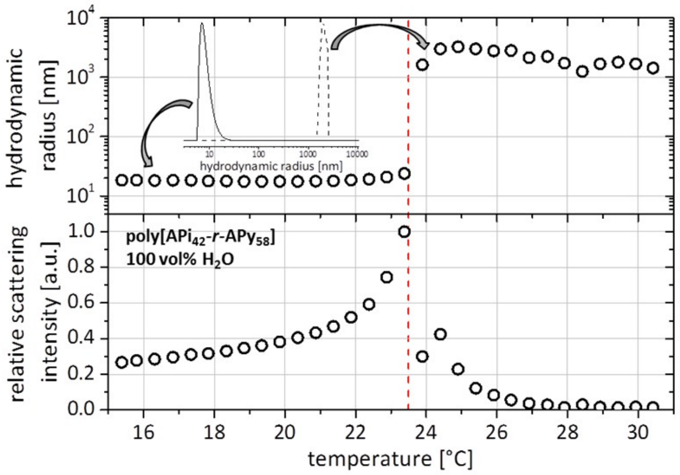

hydrodynamic radius [nm]
10^1
10^2
10^3
10^4
hydrodynamic radius [nm]
10
100
1000
10000
relative scattering intensity [a.u.]
poly[APi_{42}-*r*-APy_{58}]
100 vol% H_2O
0.0
0.2
0.4
0.6
0.8
1.0
16
18
20
22
24
26
28
30
temperature [°C]

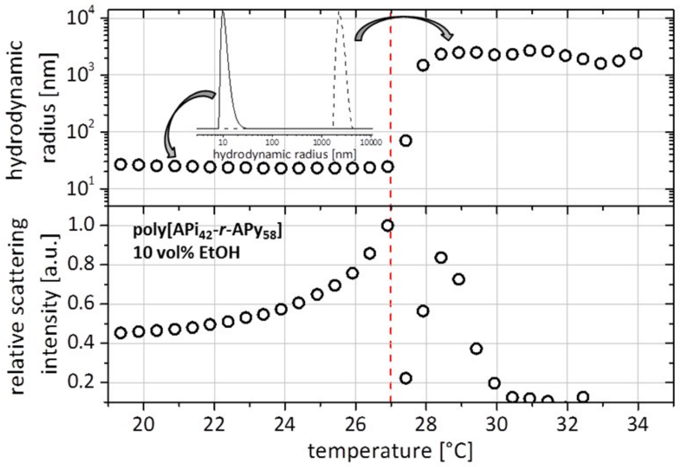

hydrodynamic radius [nm]
10^1
10^2
10^3
10^4
hydrodynamic radius [nm]
10
100
1000
10000
relative scattering intensity [a.u.]
poly[APi_{42}-*r*-APy_{58}]
10 vol% EtOH
0.2
0.4
0.6
0.8
1.0
20
22
24
26
28
30
32
34
temperature [°C]

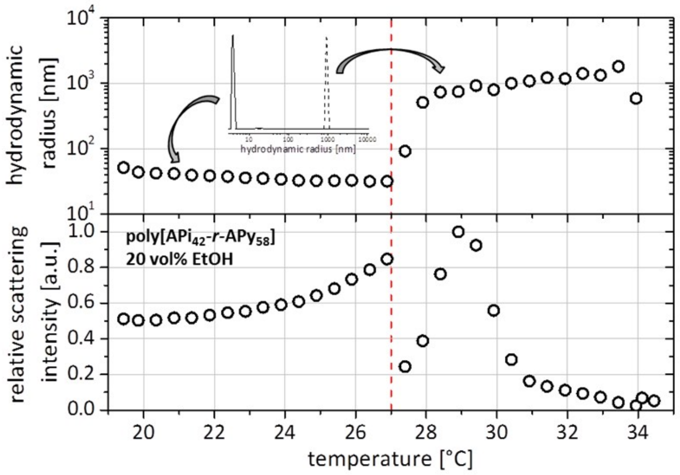

hydrodynamic radius [nm]
10^1
10^2
10^3
10^4
hydrodynamic radius [nm]
10
100
1000
10000
relative scattering intensity [a.u.]
poly[APi_{42}-*r*-APy_{58}]
20 vol% EtOH
0.0
0.2
0.4
0.6
0.8
1.0
20
22
24
26
28
30
32
34
temperature [°C]

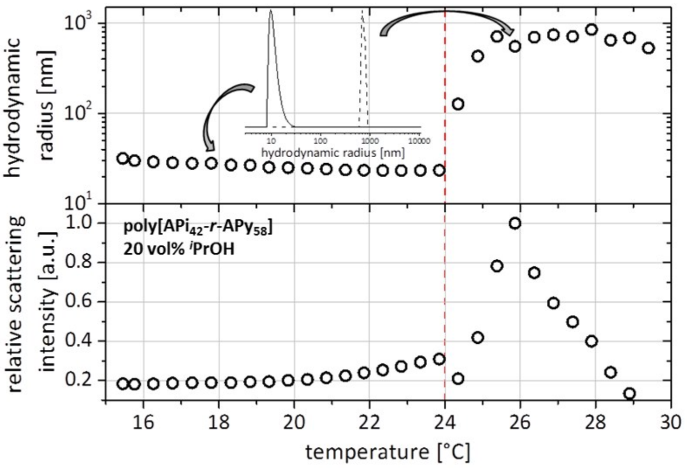

1 K.-Y. Chu and A. R. Thompson, *J Chem Eng Data*, 1962, **7**, 2.

2 Y. Tanaka, Y. Matsuda and H. Fujiwara, *J Thermophys*, 1987, **8**, 16.

3 A. S. J. Troy, *J Phys Chem*, 1946, **50**, 6.

4 C. Scherzinger, A. Balaceanu, C. H. Hofmann, A. Schwarz, K. Leonhard, A. Pich and W. Richtering, *Polymer*, 2015, **62**, 50-59.

5 D. Mukherji and K. Kremer, *Macromolecules*, 2013, **46**, 9158-9163.

6 D. Mukherji, C. M. Marques and K. Kremer, *Nat Commun*, 2014, **5**.

7 S. Eggers, B. Fischer and V. Abetz, *Macromol Chem Phys*, 2016, **217**, 735-747.

8 V. Aseyev, S. Hietala, A. Laukkanen, M. Nuopponen, O. Confortini, F. E. Du Prez and H. Tenhu, *Polymer*, 2005, **46**, 7118-7131.